

## COMBUSTION OF A SPHERICAL DIFFUSION FLAME IN A RADIATIVE FIELD

Ziji Zhang and Ofodike A. Ezekoye  
Department of Mechanical Engineering  
University of Texas at Austin  
Austin, Texas

### ABSTRACT

One methodology for modeling fire induced flow fields is based upon a Lagrangian view of the fire. Large scale processes are modeled using a Large Eddy Simulation (LES) method and are then appropriately coupled to a subgrid scale model of the small scale combustion processes. The subgrid scale combustion model utilizes Lagrangian flamelets. On the subgrid scale, detailed computations are performed to calculate the combustion history of an individual fuel element with prescribed initial conditions. In this paper, the soot evolution and burning characteristics within a spherical diffusion flame element are phenomenologically modeled and the possibility of radiation quenching for certain soot loadings is noted. A comparison is made between finite rate chemistry effects and fast or diffusion-limited chemistry results.

### NOMENCLATURE

$a$	fuel mass fraction dependent exponent in reaction rate
$a_p$	Planck mean absorption
$A$	pre-exponential constant of reaction rate
$b$	oxygen mass fraction dependent exponent in reaction rate
$c_p$	specific heat capacity
$C_2$	Planck's second constant
$D_i$	mass diffusivity of species $i$
$E_a$	activation energy
$f_v$	soot volume fraction
$h_i$	heat of formation of species $i$
$k$	thermal conductivity
$p$	pressure
$q_r$	radiative heat flux
$r$	radial coordinate
$r_o$	initial fuel dimension of thermal element
$\bar{R}$	universal gas constant
$S_i$	source term in the $i$ th species conservation equation

$t$	time
$T$	temperature
$u$	velocity
$Y_i$	mass fraction of species $i$
$W_i$	molecular weight of species $i$

### Greek Symbols

$\alpha$	thermal diffusivity
$\beta$	soot effective loading parameter
$\gamma$	stoichiometric ratio
$\nu$	kinematic viscosity
$\rho$	density
$\sigma$	Stefan-Boltzmann constant
$\dot{\omega}_i$	reaction rate of species $i$
$\varsigma$	fuel dependent radiative constant

### Subscripts

$f$	fuel
$fl$	flame
$n$	related to nitrogen species
$o$	related to oxygen species
$s$	associated with soot
$sg$	soot generation
$so$	soot oxidation
$T$	thermophoretic
$\infty$	ambient

### INTRODUCTION

An obstacle to the accurate simulation of the combustion processes in various turbulent combustion phenomena is the inability to model all scales of interactions on the computational grid. Several modeling strategies are presently used to overcome this obstacle (Bilger, 1989). The laminar flamelet approach to combustion appears to provide a means of resolving many of the complexities associated with turbulent combustion. Unfortunately however, problems exist with the temporal and spatial temperature and soot species specifications in heavily sooting and radiating flames (Jang et al., 1992).

Ideally, any turbulent combustion process should be solved in such a way that the grid resolution is adaptive and provides

sufficient resolution for the combustion/reaction processes while requiring less accurate resolution of the large scale convective processes. A Lagrangian formulation of the laminar flamelet approach may circumvent some of the difficulties associated with present turbulent combustion calculations (Baum et al., 1994).

One might imagine a Lagrangian method of combustion in which computational fuel elements are released into the large scale flow field. This concept may be justified since the singular issue in most turbulent combustion calculations is the "bookkeeping" of the fuel species through oxidation. A coarse grid Eulerian calculation is used to specify the mean mixture fraction (or extent of mixing with air that any individual fuel element undergoes). The coarse grid Eulerian calculation may also prescribe the local turbulence levels (scalar dissipation) at the location of any material element that originated as fuel species. A computation/look-up table from the element specifies the reaction rate, the amount of fuel remaining, the amount of various products generated from the initial mass of fuel, and the amount of soot generated by the initial mass of fuel. The temperature field may be computed on the Eulerian grid using the heat release rates of the small elements as source terms.

Investigations of Lagrangian flamelet based combustion have been conducted by Marble (1985), Karagozian and Marble (1985), Gore et al. (1992), and Atreya and Agrawal (1993), Mauss et al. (1990). In a previous study, we examined the feasibility of a thermal element model of fires using a fast chemistry (diffusion-limited) model of the thermal element combustion processes. A global soot evolution parameter,  $\beta$ , was used to describe the rate of formation of soot as a fraction of the rate of consumption of the fuel. In this study, the fast chemistry limit is replaced by a finite rate chemistry model, and the soot source and sink terms are phenomenologically modeled. The phenomenological soot model is evaluated by comparisons with the models of Kennedy et al. (1990), and Moss, et al. (1988). Comparisons are also made with the model of Atreya and Agrawal (1993), who modeled a planar analogy of the spherically symmetric problem.

The model that is detailed within this paper is also applicable to analyzing the new body of work on microgravity flames. Under microgravity conditions, the symmetry inherent to our model would be valid over many size ranges of flames. It is interesting to note that under normal gravity conditions that such symmetry is also achievable for large Froude number diffusion flame combustion as shown by Ban et al. (1992). Physically, situations where there are negligible buoyancy forces possess interesting possible flame configurations. In particular, the possibility exists for a fuel element to be mixed with products of combustion. The thermal element model is used to evaluate the effects of dilution of the thermal element burning history by varying the amounts of combustion products (including soot) dilution of the element.

### THERMAL ELEMENT MODEL

The thermal element is envisioned to be a spherically symmetric fuel-air element. The equations governing a thermal element reaction are

$$\frac{\partial(\rho r^2)}{\partial t} + \frac{\partial(u \rho r^2)}{\partial r} = 0 \quad (1)$$

Species conservation

$$\frac{\partial(\rho r^2 Y_i)}{\partial t} + \frac{\partial(u \rho r^2 Y_i)}{\partial r} = \frac{\partial}{\partial r} \left( r^2 \rho D_i \frac{\partial Y_i}{\partial r} \right) + S_i r^2 \quad (2)$$

where  $i=1 \dots N$ ,  $N$  is the number of species in the system  
Soot species evolution is included and the soot mass conservation equation has the form

$$\frac{\partial(\rho r^2 Y_s)}{\partial t} + \frac{\partial((u + u_T) \rho r^2 Y_s)}{\partial r} = \frac{\partial}{\partial r} \left( r^2 \rho D_s \frac{\partial Y_s}{\partial r} \right) + S_s r^2 \quad (3)$$

The thermophoretic velocity in the soot mass conservation equation is specified by (Talbot et al., 1980)

$$u_T = -0.55 \left( \frac{\nu}{T} \frac{\partial T}{\partial r} \right)$$

Energy conservation is specified as

$$\frac{\partial(\rho r^2 c_p T)}{\partial t} + \frac{\partial(u \rho r^2 c_p T)}{\partial r} = \frac{\partial}{\partial r} \left( r^2 \left( k \frac{\partial T}{\partial r} + q_r \right) \right) + \sum_{i=1}^N h_i \omega_i r^2 \quad (4)$$

The divergence of the radiative flux vector is modeled as

$$\frac{\partial q_r}{\partial r} = -4 a_p \sigma (T^4 - T_\infty^4)$$

where the Planck mean absorption is calculated to be

$$a_p = \frac{4 \zeta \nu T}{C_2}$$

where  $\zeta$  is a fuel dependent constant and  $C_2$  is Planck's second constant (Siegel and Howell, 1981).  $\nu$  is soot volume fraction. The initial and boundary conditions for the system of conservation equations are

$$\left. \begin{array}{l} Y_f = 1, \sum_{i \neq f} Y_i = 0 \quad @ \quad r \leq r_o \\ Y_f = 0, \sum_{i \neq f} Y_i = 1 \quad @ \quad r > r_o \end{array} \right\} @ \quad t = 0$$

$$\frac{\partial Y_i}{\partial r} = \frac{\partial T}{\partial r} = 0 \quad @ \quad r = 0$$

$$\frac{\partial Y_i}{\partial r} = \frac{\partial T}{\partial r} = 0 \quad @ \quad r \rightarrow \infty$$

For the short time scales (order .1 seconds) associated with the burnout of a fuel element, viscous effects are negligible and the velocity is specified only as the potential component of the true velocity field. The potential component is determined by mass conservation requirements.

The ideal gas assumption is used and the pressure is assumed to be constant in both space and time. The ideal gas equation of state is

$$\rho = \frac{p}{\bar{R} T \sum_{i=1}^N \frac{Y_i}{W_i}} \quad (5)$$

where  $\bar{R}$  is the universal gas constant. The mass fraction of the  $N$ th species satisfies

$$Y_N = 1 - \sum_{i=1}^{N-1} Y_i \quad (6)$$

By using the following definitions

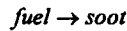
$$\tilde{T} = \frac{T}{T_f}, \quad \tilde{t} = \frac{t\alpha_f}{R_o^2}, \quad \tilde{\rho} = \frac{\rho}{\rho_f}, \quad \tilde{\alpha} = \frac{\alpha}{\alpha_f}$$

$$\tilde{r} = \frac{r}{R_o}, \quad \tilde{u} = \frac{uR_o}{\alpha_f}, \quad \tilde{c}_p = \frac{c_p}{c_{pf}}, \quad \tilde{k} = \frac{k}{k_f}$$

equations (1) through (5) are nondimensionalized. The equations are solved in terms of the nondimensional parameters by a control volume finite-difference scheme (Patankar, 1980).

### CHEMICAL REACTION RATE

A global (phenomenological) reaction mechanism with soot formation and destruction steps is formulated as follows:



Four species equations are solved in the model: fuel, oxygen, soot, and nitrogen. The product mass fraction is specified by mass conservation constraints. The source/sink terms corresponding to the fuel, oxygen, soot, and nitrogen evolution equations are presented respectively as

$$S_f = -\dot{\omega}_f - \dot{\omega}_{sg}$$

$$S_o = -\gamma\dot{\omega}_f - \dot{\omega}_{so}$$

$$S_s = \dot{\omega}_{sg} - \dot{\omega}_{so}$$

$$S_n = 0$$

,where  $\gamma$  is the stoichiometric coefficient.

Reaction rates are specified by an Arrhenius formulation and are

$$\dot{\omega}_f = A \exp\left(-\frac{E_a}{RT}\right) Y_f^a Y_o^b \rho^{a+b} \quad (7)$$

$$\dot{\omega}_{sg} = A_{sg} \exp\left(-\frac{E_{asg}}{RT}\right) Y_f \rho \quad (8)$$

$$\dot{\omega}_{so} = A_{so} \exp\left(-\frac{E_{aso}}{RT}\right) Y_o Y_s \rho^2 \quad (9)$$

### RESULTS AND DISCUSSION

With no soot production, the global dynamics of a flame modeled by a finite rate chemistry model and a fast chemistry model are quite similar. The total burnout time for the finite rate chemistry model formulation is dependent on the reaction rate specification. In this study, several single step fuel oxidation rates were examined. With no soot, the burnout time depended on the reaction order specification, but was relatively insensitive to other reaction rate parameters (i.e., activation energy, and pre-exponential term). Nominally, propane was specified as the fuel. A one step propane mechanism specified by Westbrook and Dryer (1981) has proven to characterize many aspects of premixed flame propagation (Ezekoye et al. 1992). Westbrook and Dryer noted that the choice of reaction order in premixed flame applications was essential to the accurate computation of fuel rich combustion properties; for propane combustion they chose 1.75 as the reaction order. The results of their one step mechanism in a diffusion flame application were examined by comparison with a fast chemistry formulation and also with the more often used second order reactions. As it is seen in figure 1, the Westbrook and Dryer reaction rate predicts fuel burnout 25% faster than second order reactions with similar magnitude pre-exponential terms. The second order reaction mechanism was chosen in order to make this work more generalizable. For the range of parameters that are examined, the nondimensional burnout time varied between 7.3 and 9.6.

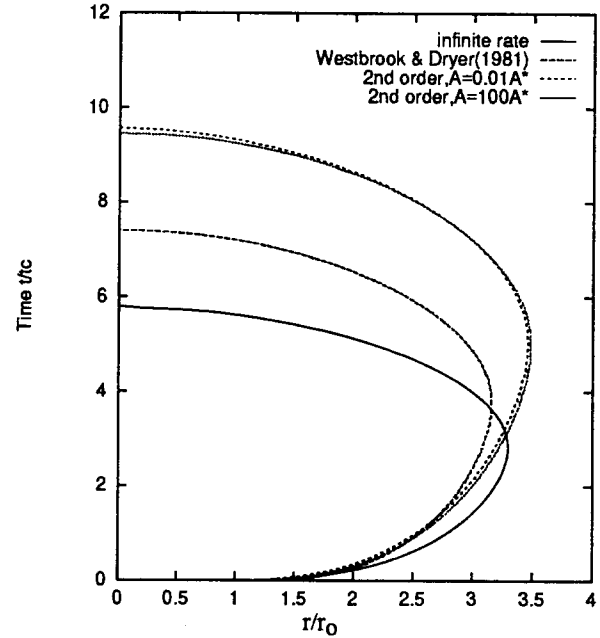


FIGURE 1. COMPARISON OF FLAME SHEET TRAJECTORY FOR DIFFERENT REACTION RATES.

In a previous formulation, the soot production rate was specified to be a fraction,  $\beta$ , of the fuel consumption rate. That formulation did not provide the possibility for soot oxidation. Any soot that was created remained within the element  $\beta$  for all time. An equivalent definition of the soot loading factor, is the final mass of soot divided by the initial amount of fuel. In the fast chemistry limit, it is possible to specify the radiative strength of any given element in terms of its size and also its soot loading factor. As presented in the finite rate chemistry model description, the soot evolution source and sink terms are now specified by Arrhenius reaction rates dependent on the fuel mass fraction, soot mass fraction, and oxygen mass fractions. There is not a soot loading factor that can be based on rates of soot production and fuel consumption. Since the oxidation term can destroy any soot that participated in the radiation process, the definition of the soot loading factor in terms of the final mass of soot divided by the initial mass of fuel did not seem appropriate and unique. Thus,  $\beta$  is specified in terms of the average mass of soot during the combustion process divided by the initial mass of fuel. Results of the soot mass as a function of time for different overall soot loadings are presented in figure 2. The pre-exponential term for the soot generation reaction was changed in order to get different  $\beta$  values. For the lowest  $\beta$  case, the soot is fully oxidized at the end of the combustion process. It is noted that the final time for the heavy soot loading flame is approximately 20% longer than the burnout time for the low loading cases. This result is more clearly seen in figure 3 where the flame sheet (defined by the maximum reaction rate) trajectory is presented for the three soot loadings.

From figure 3 it is also seen that the lower soot loading maximum reaction rate (i.e., flame location) extends further out spatially than the heavy loading case. Both the longer burnout time and the smaller expansion of the heavily loaded case are due

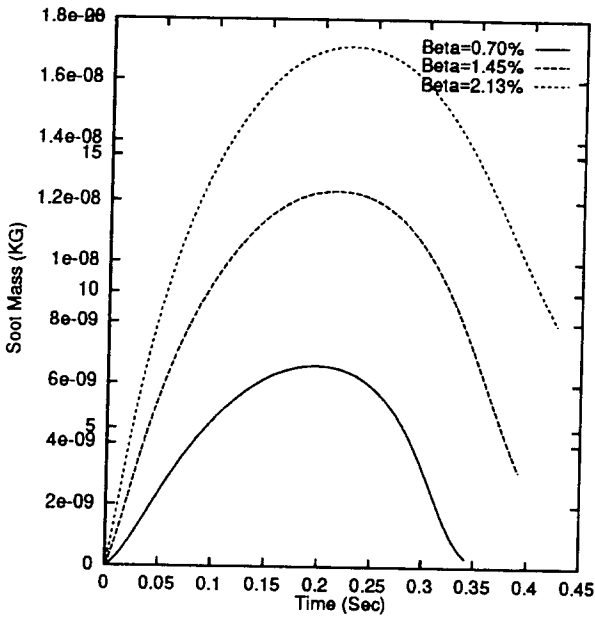


FIGURE 2. SOOT MASS VERSUS TIME FOR DIFFERENT SOOT LOADING PARAMETERS.

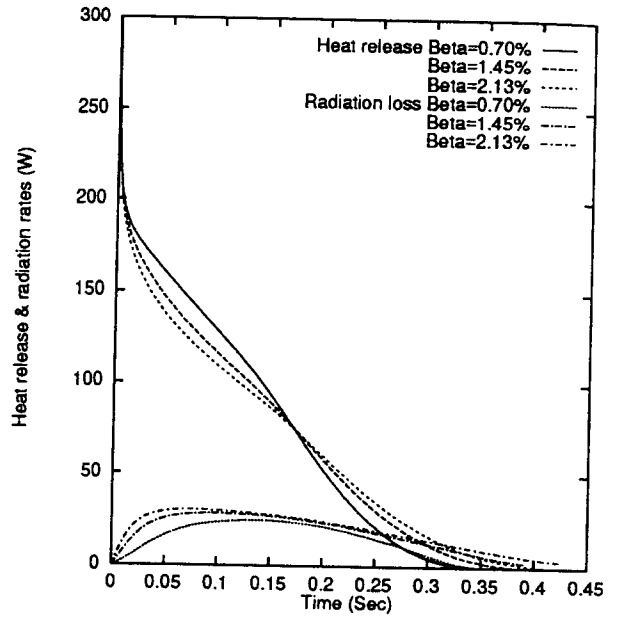


FIGURE 4. HEAT RELEASE & RADIATIVE LOSS RATES FOR DIFFERENT SOOT LOADING PARAMETERS.

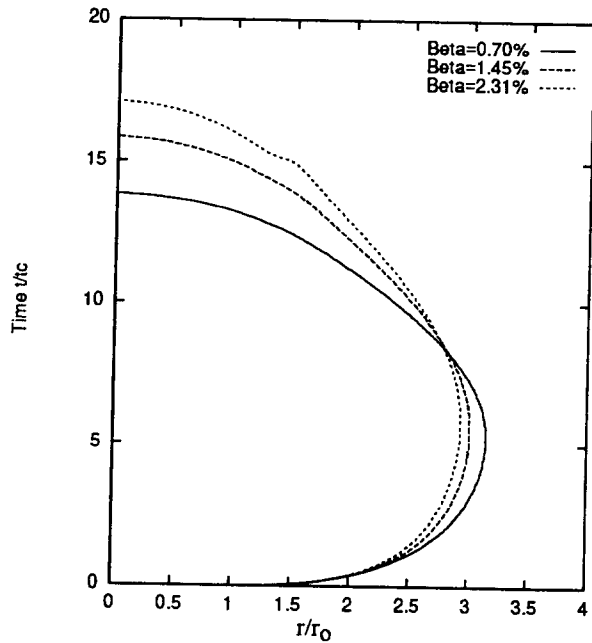


FIGURE 3. FLAME SHEET TRAJECTORY FOR DIFFERENT SOOT LOADING PARAMETERS.

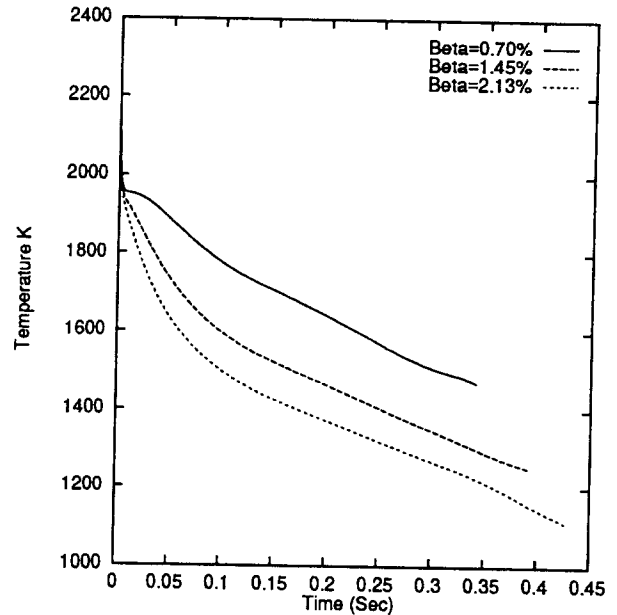


FIGURE 5. SOOT AVERAGE TEMPERATURE VERSUS TIME FOR DIFFERENT SOOT LOADING PARAMETERS.

to the lower average temperature of the heavily loaded element. In figure 4, the total heat release and the radiative heat transfer rate for the three  $\beta$  cases are shown. Although the soot average mass of the heavily loaded case is over three times larger than that of the lightly loaded element, the total energy radiated (i.e., the integrated heat transfer rate) is only 52% larger. The radiative loss fractions (total radiated energy divided by chemical energy) for the three  $\beta$  values (0.70%, 1.45%, and 2.13%) are 19%, 26%, and 30% respectively. Again, the average temperature of the element, and the average temperature of the

soot are significantly lower for high  $\beta$  flames as compared to low  $\beta$  flames that the total radiative output does not vary significantly with respect to  $\beta$ . The average soot temperatures are presented in figure 5.

For  $\beta = 2.13\%$ , the soot volume fraction is shown in figure 6 in mixture fraction space. The soot species primarily exists between a mixture fraction of 0.05 and unity (i.e., on the fuel side of the flame sheet). At early times, the temperature is near the adiabatic flame temperature for a mixture fraction range between

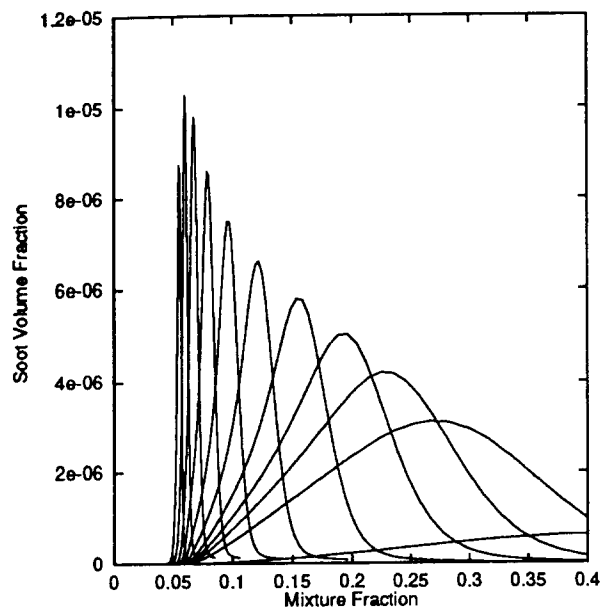


FIGURE 6. SOOT VOLUME FRACTION VERSUS MIXTURE FRACTION FOR  $\beta = 2.13\%$ .

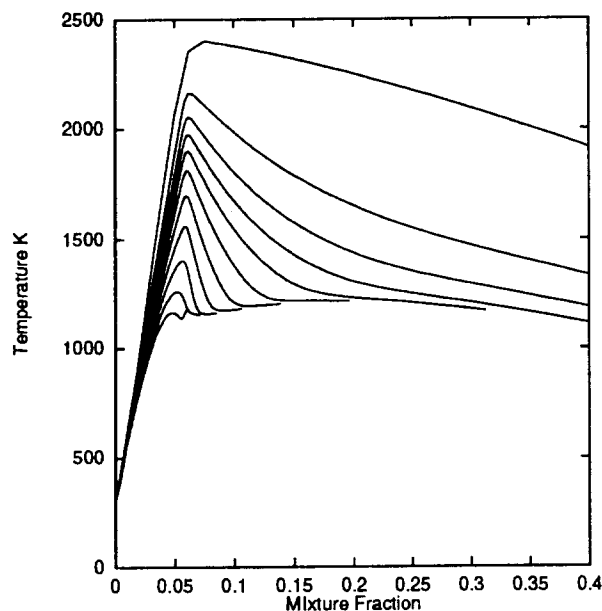


FIGURE 7. TEMPERATURE PROFILE VERSUS MIXTURE FRACTION FOR  $\beta = 2.13\%$ .

0.05 and 0.6. The soot generation rate is specified as an Arrhenius pyrolysis step which depends solely on the fuel species. Thus, for large fuel concentrations at high temperatures, soot species was produced at relatively large values of the mixture fraction (e.g., 0.5). At later times, the soot at the core of the element has reduced the gas temperature sufficiently that soot production rates in these high fuel concentration regions have diminished. The peak volume fractions shift towards the flame sheet ( $Z=0.05$ ). At some point, depending on how much soot oxidation takes place, the peak soot volume fraction begins to decrease due to oxidation reactions. These trends appear to be

consistent with the work of Moss et al. (1988) in which an ethylene-air diffusion flame is modeled and compared with experimental results from a Wolfhard-Parker burner. They plot the soot volume fraction in mixture fraction space at three downstream locations. Their figure indicates that the soot volume fraction profile thins, peaks downstream, and shifts towards smaller mixture fraction values. The time variable in this study compares to their downstream length variable. As is typically noted in sooting diffusion flames, the soot peaks near the flame sheet (i.e.,  $Z = 0.05$ ) tend to act as an enthalpy sinks and produce a nonlinear temperature profile on the fuel side in mixture fraction space (figure 7).

Atreya and Agrawal (1993) found that soot oxidation and soot radiation effects balanced each other in terms of magnitude in their study of a planar diffusion flame. In figure 8, the radiation heat transfer rate and soot oxidation heat release rates are plotted versus time for three soot loadings. It is found that the radiative heat transfer rates in the present geometry (i.e., a spherical flame) are much larger initially than the heat release rates associated with soot oxidation. At later times, the oxidation heat release rate and the radiative heat transfer rates are comparable. Physically, the soot is produced on the fuel side of the flame at early times and does not begin to oxidize until the flame begins to burn backwards consuming the remaining fuel. An OH based oxidation mechanism is utilized by Agrawal and Atreya while a molecular oxygen oxidation mechanism is assumed in this work. The model by the aforementioned authors would allow soot oxidation on the fuel side of the flame by equilibrium or super-equilibrium hydroxyl radicals. As there is no consensus in the literature on the relative contribution of OH soot oxidation relative to  $O_2$  oxidation, the  $O_2$  route is chosen (Leung et al. 1991); it is also less ambiguous to specify the amount of molecular oxygen in the flame than the amount of hydroxyl radical.

In the spirit of developing a phenomenological model, the effects of many physical parameters were examined within the model formulation. Among these, it was noted that for very reasonable values of the activation energy for the fuel reactions ( $E_a = 42$  kcal/mole) and also for the soot reactions ( $E_{asg} = E_{aso} = 38$  kcal/mole) that radiative extinction of the flame could be established. For sufficiently large activation energies, it is clear that any flame can be quenched with very little soot loading. In the presence of product dilution, it was found that when using large enough activation energies that the flame could not be ignited; after several time steps the reaction rate would go to zero. For moderate activation energies it was found that with an initial uniform soot dilution of 1 ppm that a peak soot volume fraction of approximately 11 ppm was sufficient to extinguish the flame (see Table 1). In figure 9 the flame trajectory is shown for a quenching and non-quenching cases corresponding to Table 1. Since the flame location is specified by the maximum reaction rate within the flame, it is somewhat arbitrary to pick out the time of quenching from the flame trajectory profile. One does note that an abrupt transition in the location of the maximum reaction rate occurs at the dimensionless time value of approximately 11.5. In agreement with the reports by Wichman (1994), the extinction process occurs for weak flames (most of the fuel has been consumed) in which the soot shell begins to cross over the reaction zone from the fuel side to the oxidant side. A less ambiguous indicator that flame quenching occurs is provided by the heat release rate. At the moment of quenching, the heat release rate goes to zero.

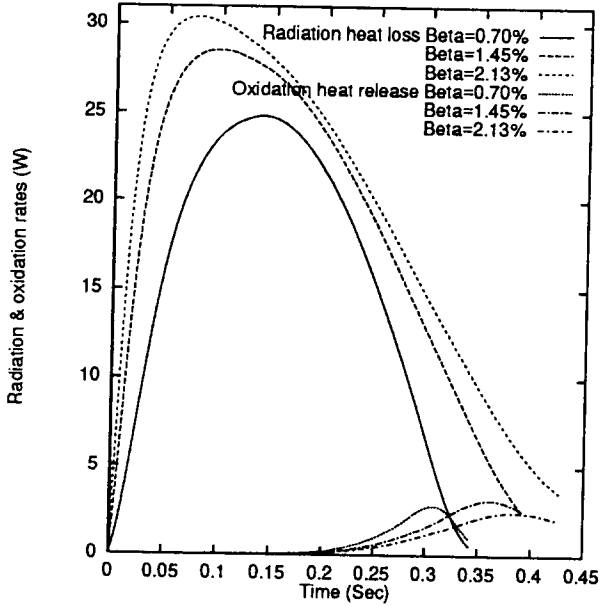


FIGURE 8. RADIATIVE LOSS AND SOOT OXIDATION RATES FOR DIFFERENT SOOT LOADING PARAMETERS.

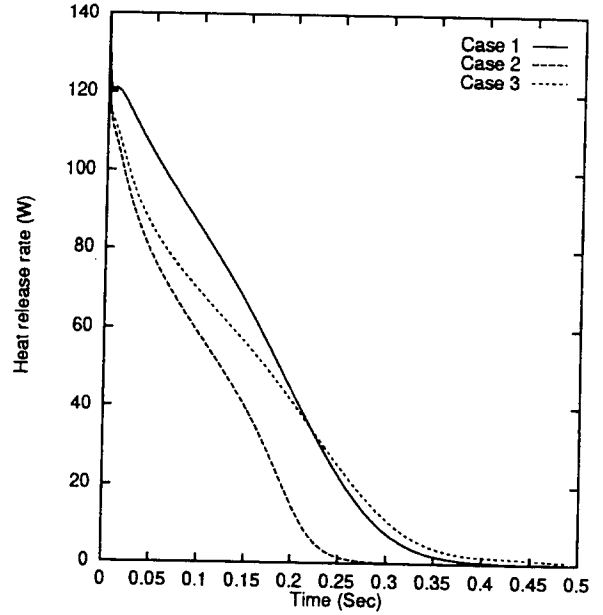


FIGURE 10. HEAT RELEASE RATES FOR 3 CASES WITH INITIAL PRODUCT DILUTION.

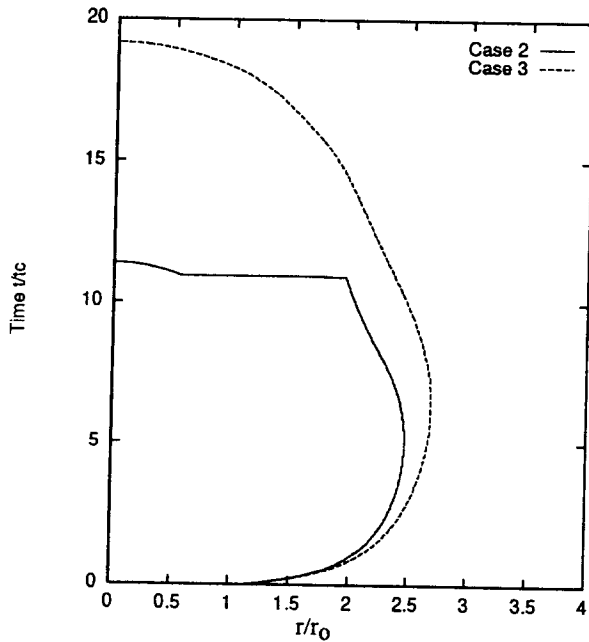


FIGURE 9. FLAME SHEET TRAJECTORY FOR 2 CASES WITH INITIAL PRODUCT DILUTION.

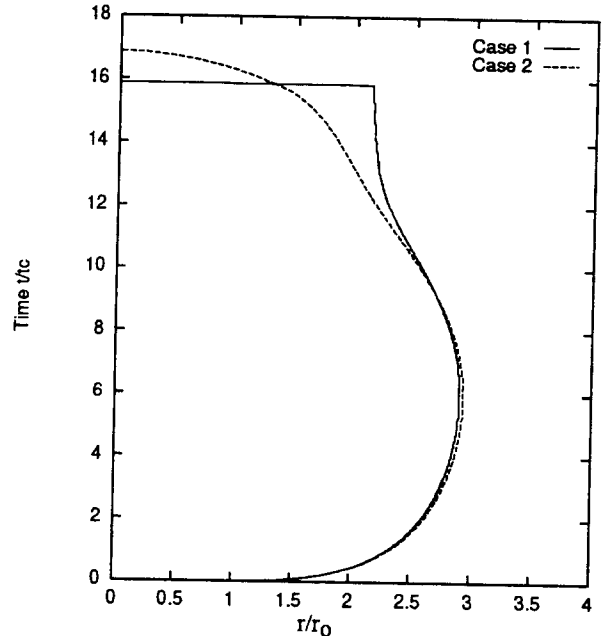


FIGURE 11. FLAME SHEET TRAJECTORY FOR 2 CASES WITHOUT INITIAL PRODUCT DILUTION.

It is noted that total heat release for quenching (case 2) is less than that for no-quenching (cases 1 and 3) as shown in figure 10. Three no-dilution cases in which the soot generation and oxidation rates are varied to induce quenching are shown in Table 2. The flame sheet trajectories corresponding to cases 1 and 2 in Table 2 are plotted in figure 11. In general, for cases with dilution, a larger pre-exponential term ( $A_{sg}$ ) is required to force quenching (Table 1) as compared to quenching cases with no-dilution (Table 2). Cases with initial soot and product dilution have lower average temperatures and thus lower generation rates of soot. In order to match the peak soot volume fractions

associated with quenching (i.e., 11 ppm) the generation rates must be artificially increased. Peak soot volume fractions associated with radiative quenching are consistent with data from heavily soot loaded flames. It is noted that flames with identical soot generation rates and peak volume fractions may or may not quench because of different oxidation rates. The total hot soot mass appears to be the dominant criteria for quenching.

Case	$A_{sg}$	$A_{so}$	$f_v$	quenching
1	$20A_{sg}^*$	$0.2A^*$	$2.5 \cdot 10^{-6}$	no
2	$200A_{sg}^*$	$0.0002A^*$	$1.2 \cdot 10^{-5}$	yes
3	$200A_{sg}^*$	$20A^*$	$1.2 \cdot 10^{-5}$	no

$$A_{sg}^* = 3.53 \cdot 10^5$$

Case	$A_{sg}$	$A_{so}$	$f_v$	quenching
1	$20A_{sg}^*$	$0.01A^*$	$1.1 \cdot 10^{-5}$	yes
2	$20A_{sg}^*$	$20A^*$	$1.1 \cdot 10^{-5}$	no
3	$20A_{sg}^*$	$100A^*$	$1.1 \cdot 10^{-5}$	no

## CONCLUSIONS

A basic flame geometry that is relevant to microgravity combustion and subgrid scale combustion modeling is characterized in terms of simple phenomenological models which display a variety of phenomena. It is shown that nonsmoking (i.e., fully oxidized soot) flames may have significant radiative loss fractions depending on the time (axial location downstream) in the flame history that the soot is oxidized. The time variable used in this study is analogous to the downstream distance in a steady jet flame. Molecular oxygen oxidation of the soot species was found to occur late in the element burning history and then balanced the soot radiation. By lumping the actual soot inception and growth processes into a single evolution equation with soot generation and oxidation, it was found that an initial soot dilution of a flame could serve to maintain the flame temperatures sufficiently low such that further significant soot production was unlikely; it is improbable that such a result would remain valid if a more sophisticated treatment of the soot chemistry were used. An initial soot dilution would provide an extremely large surface area for soot growth processes. However, it is conceivable that this result would remain valid for a non-carbon based solid radiating diluent species injected into the fuel and air streams. For weak flames in which the amount of fuel species is small radiative quenching of the reaction was observed.

## ACKNOWLEDGMENTS

This work is supported by the National Institute of Standards and Technology (NIST) under Grant No. 60NANB3D1436.

## REFERENCES

Atreya, A. and Agrawal, S., "Effect of Radiative Heat Loss on Diffusion Flame in Quiescent Microgravity Atmosphere", presented at NIST Annual Conference on Fire Research, NISTIR 5282, pp.21-22, 1993.

Ban, H., Venkatesh, S., and Saito, K., "Momentum-Diffusion Controlled Laminar Diffusion Flame", HTD-Vol. 223, pp.127-133, Heat and Mass Transfer in Fire and Combustion Systems, ASME 1992.

Baum, H.R., Ezekoye, O.A., McGrattan, K.B., and Rehm, R.G., "Mathematical Modeling and Computer Simulation of Fire Phenomena", Theoretical and Computational Fluid Dynamics, in press 1994.

Ezekoye, O.A., Baum, H.R., and Rushmerier, H.E., "A Thermal Element Model of Fires", submitted to Combustion and Flame, 1994.

Ezekoye, O.A., Greif, R., and Sawyer, R.F., "Increased Surface Temperature Effects on Wall Heat Transfer During Unsteady Flame Quenching", Twenty-Fourth Symposium (International) on Combustion/The Combustion Institute, pp. 1465-1472, 1992.

Gore, J.P. and Jang, J.H., "Transient Radiation Properties of a Subgrid Scale Eddy", ASME Journal of Heat Transfer, Vol 114, 1992.

Karagozian, A.R. and Marble, F.E., "Study of a Diffusion Flame in a Stretched Vortex", Combustion Science and Technology, Vol. 45, 1985.

Kennedy, I.M., Kollmann, W., and Chen, J.Y., "A Model for Soot Formation in a Laminar Diffusion Flame", Combustion and Flame, Vol. 81, pp.73-85, 1990.

Leung, K. M., Lindstedt, R.P., and Jones, W.P., "A Simplified Reaction Mechanism for Soot Formation in Nonpremixed Flame", Combustion and Flame Vol. 87, pp.289-305, 1991.

Marble, F.E., "Growth of a Diffusion Flame in the Field of a Vortex", Recent Advances in Aerospace Science (C. Cassci ed.), 1985.

Moss, B.J., Stewart, C.D., and Syed, K.J., "Flowfield Modeling of Soot Formation at Elevated Pressure", Twenty-second Symposium (International) on Combustion/The Combustion Institute, pp.413-423, 1988.

Mauss, F., Keller, D., and Peters, N., "A Lagrangian Simulation of Flamelet Extinction and Re-ignition in Turbulent Jet Diffusion Flames," Twenty-Third Symposium (International) on Combustion/The Combustion Institute, pp 693-698, 1990.

Patankar, S.V., Numerical Heat Transfer and Fluid Flow. Taylor and Francis, Philadelphia, 1980.

Siegel, R. and Howell, J.R., Thermal Radiation Heat Transfer. Hemisphere Publishing Company, 1981.

Talbot, L., Cheng, R.K., Schefer, R.W., and Willis, D.R., "Thermophoresis of Particles in a Heated Boundary Layer", J. Fluid Mechanics, Vol. 101, pp.737-758, 1980.

Westbrook, C.K. and Dryer, F.L., "Simplified Reaction Mechanisms for the Oxidation of Hydrocarbon Fuels in Flames", Comb. Sci. and Tech., Vol. 27, pp.31-34, 1981.

Wichman, I.S., "On the Influence of a Fuel Side Heat-Loss ('Soot') Layer on a Planar Diffusion Flame," Combustion and Flame, 97, 1994